# 3D focusing of nanoparticles in microfluidic channels

H. Morgan, D. Holmes and N.G. Green

**Abstract:** Dynamic focusing of particles can be used to centre particles in a fluid stream, ensuring the passage of the particles through a specified detection volume. This paper describes a method for focusing nanoparticles using dielectrophoresis. The method differs from other focusing methods in that it manipulates the particles and not the fluid. Experimental focusing is demonstrated for a range of different particle types, and discussed in terms of the operational limits of the device. Dynamic numerical simulations of the particle motion in the device are presented and compared with the experimental results. The potential of the device for nanoparticle control and manipulation in microfluidic chips is discussed.

## 1 Introduction

The design and fabrication of microchips for particle and molecule handling systems has experienced rapid development recently, with the aim of developing fast particle counting, analysis and sorting systems. One example of a particularly important application is the development of a flow cytometer on a chip [1–10]. For such systems to work efficiently, it is important to be able to confine the sample into a small, spatially well-defined volume, giving as small a probe volume as possible for the detector. Confining the sample to the centre of the channel also ensures that all the particles move at a constant velocity. It also eliminates signal interference from the chamber wall, as well as particle–wall interactions.

Hydrodynamic focusing or sheath flow focusing has been used to confine particles within a certain volume of a fluid stream. In this case, the sample stream is confined by flows which intersect from the sides, forming a sheath of liquid around the sample stream and confining the particles into a narrow beam. These flows can be generated using DC electrokinetic methods or using hydrostatic pressure gradients. Altering the ratio of flow rates between the sample and sheath flows alters the width of this beam, a principle which has been used by a number of groups to focus particles [e.g. 8, 9]. However, this technique has drawbacks: focusing is relatively easy to achieve in one dimension, but complex fabrication schemes are required to achieve two-dimensional focusing [6, 7]. For this to work, very accurate control of flow rates is required, and since this type of focusing acts on the fluid rather than the particles, small particles and molecules can diffuse from the sample stream into the sheath.

DC electric fields can be used to confine both the particles and the fluid into a beam using the well-known techniques of electro-osmosis and electrophoresis. Jacobson and Ramsey [9] described a device which was microfabricated from etched glass and demonstrated two-dimensional confinement of molecules with applied voltages of 3 kV. Schrum *et al.* [2] showed how electrokinetic focusing could be used to focus 0.97 μm and 1.94 μm diameter latex particles at velocities of 1 mm $s^{-1}$. Chou *et al.* developed a device for detecting DNA molecules [10] and Fu *et al.* [1, 3] used a similar system to construct a microfabricated fluorescence activated cell sorter. However, the main drawback of DC electrokinetic methods is the requirement for high voltages to move the particles and or the fluid.

AC electric fields can also be used to move particles suspended in a fluid, and therefore focus particles. It has been shown that particles can be focused in three dimensions using electric field cages, and also in two-dimensions within a fluid stream [11–13]. A small channel, typically 50 μm across is microfabricated with pairs of electrodes on the top and bottom. Using negative dielectrophoresis, particles are repelled from the electrode edges and form a tight beam in the channel centre [11, 12].

In a previous paper [14] we simulated the electric field and DEP force for a channel, and from simple Newtonian mechanics estimated the time taken for a single particle of 50 nm diameter to arrive within the central 10% of a 14 μm diameter cylindrical channel. This work indicated that focusing of such nanoparticles was feasible.

In this paper, we have designed and built a microdevice to demonstrate the effective focusing of nanoparticles within a fluid stream. We have measured the focusing efficiency for different particle sizes down to 40 nm diameter, as a function of voltage for a particle velocity of 2 mm $s^{-1}$. The electric field and DEP force was numerically simulated for a rectangular channel and the behaviour of 250 particles simulated using Brownian dynamics. The dynamic particle distribution (in two dimensions) was evaluated as a function of time. It is shown experimentally that efficient focusing can be achieved for nanometric latex particles. The experimental results are compared with the simulations.

## 2 Theory

An electric field **E** induces a dipole moment across a polarisable particle. If the field is non-uniform, the



*IEE Proceedings* online no. 20031090

doi:10.1049/ip-nbt:20031090

Paper first received 1st August 2003 and in revised form 8th October 2003

The authors are with the Bioelectronics Research Centre, Department of Electronics and Electrical Engineering, University of Glasgow, Oakfield Avenue, Glasgow G12 8LT, UK

H. Morgan and D. Holmes are now with the Department of Electronics and Computer Science, University of Southampton, Southampton S017 1BJ, UK

interaction with the dipole results in a net force on the particle and the resulting movement is referred to as dielectrophoresis (DEP). In the dipole approximation, the time-averaged DEP force is given by [e.g. 15, 16]:

$$\langle \mathbf{F}_{DEP} \rangle = \pi a^3 \varepsilon_m \mathrm{Re}[f_{CM}] \nabla |\mathbf{E}|^2 \quad (1)$$

where $a$ is the particle radius, $\varepsilon_m$ is the permittivity of the suspending medium, $\nabla$ the del vector operator and $\mathrm{Re}[f_{CM}]$ is the real part of the Clausius–Mossotti factor, given by

$$f_{CM} = \frac{\varepsilon_p^* - \varepsilon_m^*}{\varepsilon_p^* + 2\varepsilon_m^*} \quad (2)$$

where $\varepsilon_m^*$ and $\varepsilon_p^*$ are the complex permittivities of the medium and particle respectively, and $\varepsilon^* = \varepsilon - j\sigma/\omega$ with $\sigma$ the conductivity, $\varepsilon$ the permittivity and $\omega$ the angular frequency. At the centre of the channel, the dipole component vanishes and only the multipoles are responsible for any DEP force [13, 17]. In this work multipoles are not considered, since very few of the particles are positioned at the absolute centre of the channel. For effective DEP focusing the particles must experience a −veDEP force; i.e. they must always be less polarisable than the suspending medium [15, 16]. For latex particles at high frequencies the Clausius–Mossotti factor is dominated by the differences in the permittivity of the particle and the fluid (2.5 compared with 80) and so the particles experience −veDEP. Therefore, high frequencies can be used to achieve effective focusing.

Equation (1) shows that the DEP force scales linearly with particle volume ($a^3$). As has been shown [11–13], it is relatively easy to focus or trap large particles such as cells in microchannels using relatively low voltages. However, in order to achieve effective focusing of nanoparticles, the magnitude of the DEP force, i.e. $\nabla|\mathbf{E}|^2$, has to be increased considerably. From simple scaling laws, it can be seen that doubling the voltage increases the force by a factor of 4, but reducing the electrode gap by 2 increases the force by a factor of 8. Therefore, we fabricated a long channel with a small electrode gap (10 μm). In addition, Brownian motion becomes a dominant effect as particle size is reduced [16, 18]. To achieve deterministic movement of particles in the channel, the displacement produced by DEP particle flux must be substantially greater than that from Brownian motion, otherwise particle focusing will not be achieved during the transit time of the particles within the channel.

## 3 Experimental setup

### 3.1 Device design

The focusing device consisted of two glass slides onto which microelectrodes were fabricated using photolithography. A diagram of the device is shown in Fig. 1*a*. The electrodes were fabricated on two identical 500 μm thick glass slides. Polyimide insulator was spun and patterned onto one slide; the two slides were brought into contact, aligned using a mask aligner and then thermally bonded. A photograph of the device and the associated fluidic and electrical connections is shown in Fig. 1*b*. The channel consists of a long funnel shaped section, which tapers to a channel 110 μm wide by 10 μm high and 5 mm long.

The −veDEP force is directed orthogonally to the electrode edges. A tapered electrode geometry at the beginning of the channel was used to ensure that as the fluid velocity increases (with decreasing channel width), the component of the DEP force directed towards the middle increases, therefore directing the particles into the centre of the channel.

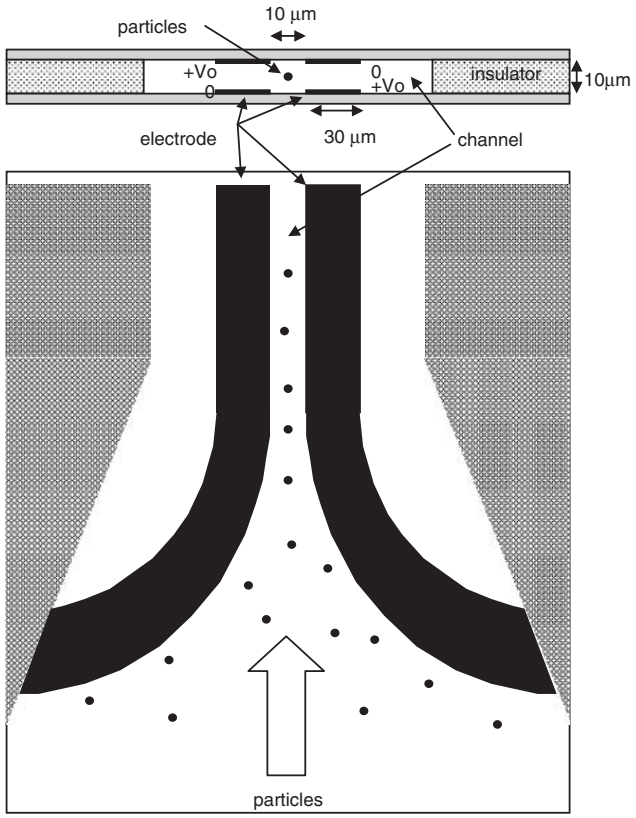


*a*

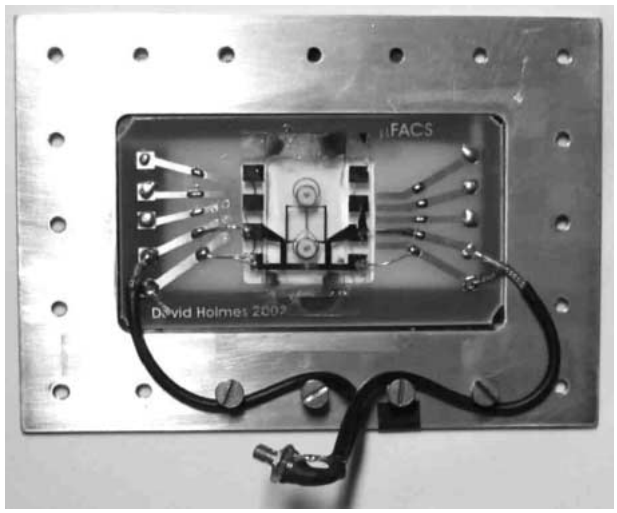


*b*

**Fig. 1** *(a) Details of focusing microchip. Electrodes in central channel are made of gold and have a gap of 10 μm, with a channel length of 5 mm; (b) Photograph of the focusing chip, which is mounted on a microscope stage to observe particle movement*

### 3.2 Experimental method

Experimental evaluation of the focusing efficiency of the device was determined using latex particles of different diameters. The particles were fluorescently loaded carboxylate-modified spheres (Molecular Probes, Oregon, USA) with a range of diameters from 40 nm to 460 nm. The particles were suspended in KCl solutions with a conductivity of approximately $10^{-4}\,\mathrm{Sm}^{-1}$. The applied AC voltages were in the range 1 to 30 V peak–peak at a frequency of 18–20 MHz. Bead images were obtained using a Zeiss Axiovert 200 fluorescence microscope, and a Hamamatsu Orca ER digital camera.

### 3.3 Numerical method

The electric potential, field and dielectrophoretic force were simulated for a cross-section similar to that of the actual device (110 μm × 10 μm) using the finite element method. Details of the method can be found in previous publications [16, 19]. In order to determine the spatial and temporal distribution of the particles, a Brownian dynamic simulation was performed using the two-dimensional force map as a reference grid. 250 particles with a uniform distribution were introduced and the position of each particle calculated as a function of time using the Langevin equation [20], with a 0.4 ms time step. In this work, given the three-dimensional nature of the problem and the relatively low density of particles, particle–particle interactions were ignored. Finally, the cross-sectional steady-state particle distribution was estimated by fitting a Gaussian profile to the distribution after a substantial period of simulated time (10 s).

## 4 Results and discussion

### 4.1 Numerical

Figure 2 shows a plot of the DEP force vectors on a lateral cross-section of the device (note that this image is stretched in the vertical direction to make the vectors clearer). The −veDEP force acts away from the electrode edges, focusing particles into the centre of the channel. There is a clear

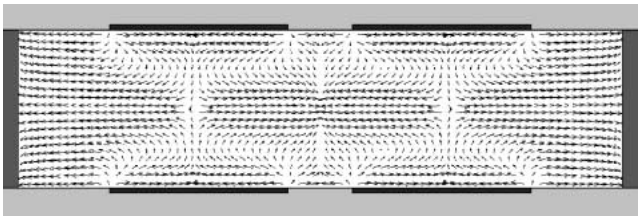

**Fig. 2** *−veDEP force vectors for the focusing device showing how particles are directed into the centre of the channel*
The electrodes (30 μm wide) are shown on the top and bottom of the channel, which is 10μm high. (Note that this diagram is not to scale)

focusing point in the centre, where the particles collect under −veDEP. Field minima are also found directly between the two opposite electrodes; particles do not collect here, but they can remain in this region because the DEP force is very weak. Also note that −veDEP can force particles to the channel wall (Fig. 3). In the actual device, the funnel electrodes ensure that all the particles are confined to the centre of the channel. In a previous design, where the insulator covered most of the electrodes, these local minima were absent [14].

Figure 3 shows seven sequential images of the simulated particle distribution as a function of time for $a = 108$ nm and applied voltage of 2.5 V peak per electrode (i.e. 10 V peak–peak on Fig. 5). At time $t = 0$, the particles are evenly distributed, and after three image ($t = 0.36$ s), the majority of the particles have been focused into the centre of the channel. In the simulation, steady-state is considered to have been reached by the final image ($t = 10$). The simulation indicates that most of the particles are pushed into the centre in a short period of time, three to four video frames. It also shows that a closed cage exists in the centre, since particles do not leave this area over the course of the simulation. A full animation of the simulation can be found at [21].

As can be seen from the images, particles are also repelled from the electrodes towards the sides of the channel. However, this does not occur in the experimental device, as

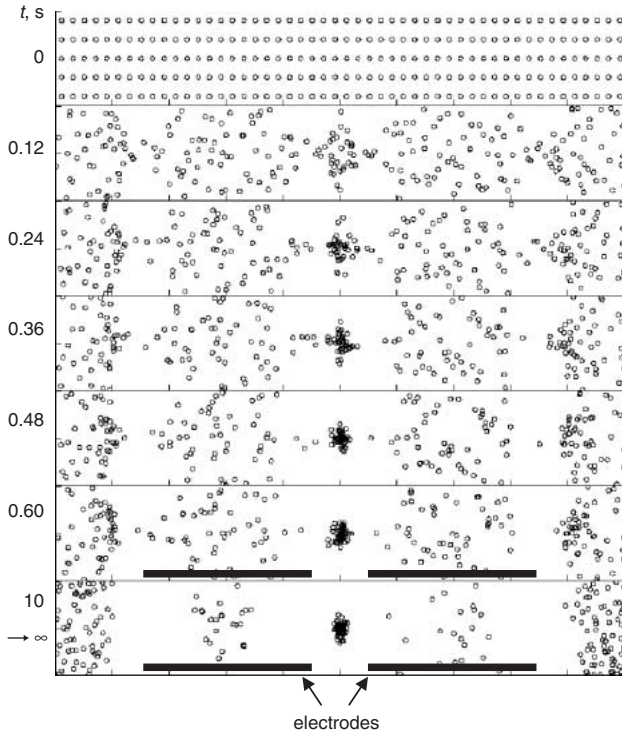


**Fig. 3** *Sequence of images from a Brownian dynamic simulation of particle behaviour with applied voltage of 10 V peak-to-peak*
At time 0s the particles are evenly distributed in the channel. Most of the focusing has been achieved within the initial 0.5 s

the funnel section pushes particles away from the sides of the channel prior to the focusing section.

Electrohydrodynamic flow can often cause unusual particle motion, particularly near electrode edges. The electrothermal flow was simulated for this device but found to be negligible, since the majority of the particles are sufficiently far from the electrode edges and also the conductivity of the solution is very low [14]. At higher conductivities, Joule heating may lead to significant electrothermal effects, particularly at the relatively high voltages used in this work.

The steady-state distributions (last image in Fig. 3) were determined for three different particle radii and six different voltages. The distribution over the final 25 time steps (1 s of time from $t = 9$ to 10 s.) were averaged and plotted against position across the channel. Figure 4 shows the results for the 216 nm diameter particles plotted for different voltages over the 4 μm region at the centre of the channel. These plots can be accurately described by a Gaussian; the width of the Gaussian ($2\sigma$) was estimated using a fitting routine in Origin 6.1, and the data plotted against voltage for the three particle sizes as shown in Fig. 5. Each curve can be represented by a single exponential fit as shown in the figure.

### 4.2 Experimental

Particles passed through the system at a constant flow rate, with a peak particle velocity (equal to maximum fluid flow velocity) of 2 mm $s^{-1}$. Particle residence time in the central channel was thus 2.5 s.

Images of the beads moving through the device were recorded on a PC (with a digital camera) and typical experimental images for 40 nm and 216 nm diameter latex particles is shown in Fig. 6*a* and *b* respectively. These pictures were obtained by summing and averaging five images taken at 200ms intervals, obtained at the midpoint of the channel (approximately 2.5 mm from the end). The images

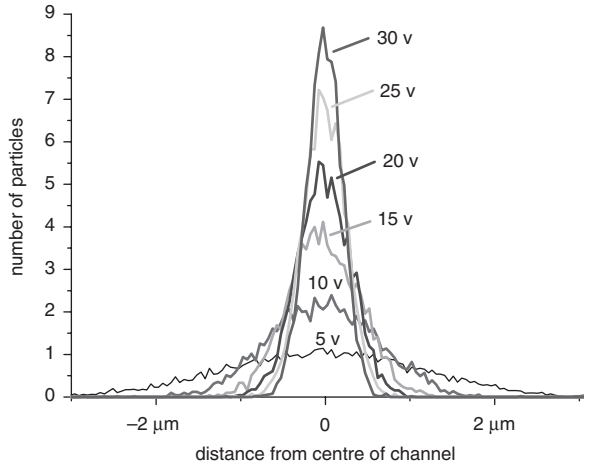


**Fig. 4** *Plot of particle distribution in central 6 μm of channel for 216 nm diameter latex particles as a function of voltage*
Simulation for 100 particles shows that peak height increases and width decreases as voltage, and hence the DEP force is increased

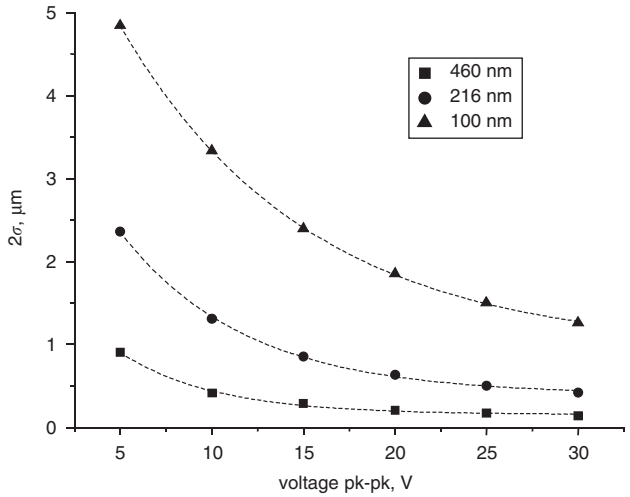


**Fig. 5** *Plot showing widths (2 σ) of Gaussian fits to the data of Fig. 4 for three different particle sizes as a function of the applied voltage*
The trends can be fitted by single exponential functions

clearly show how increasing the voltage causes the stream of particles to become focused into the centre of the channel. There was no evidence that the width of the focused particle

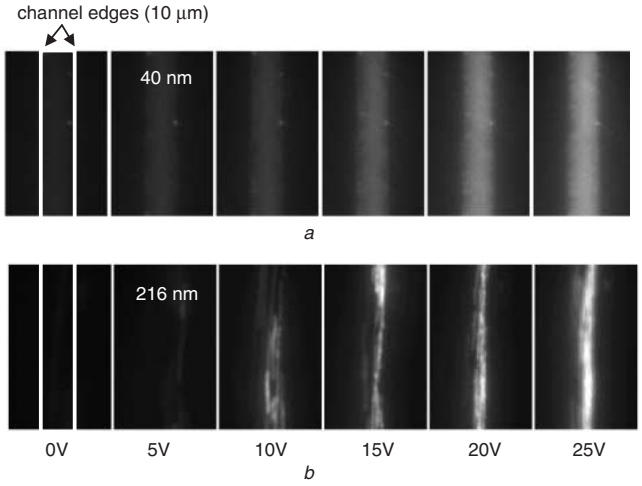


**Fig. 6** *Series of averaged images showing effect of increasing applied voltage on focusing of particles. Difference between 216 nm particles and 40 nm particles is clear*

stream varied along the length of the channel, indicating that the device achieved steady-state focusing within the first few hundred microns. This trend was confirmed from numerical simulations (Fig. 3) where it is clear that the pseudo steady-state distribution is achieved very quickly. Re-calculating the data shown in Fig. 3 after 1 s, rather than 10 s made little difference to the focusing trends.

Focusing was quantified by summing all the horizontal rows of pixels in an image along the vertical direction for a 120 μm long section of the channel at the midpoint of the channel. This was done for six or seven frames, which were collected over a duration of 1 s. The pixel number versus $x$-coordinate (across the channel) data is shown in Fig. 7 for 40 nm and 216 nm diameter particles for three different applied voltages. These curves were fitted to a Gaussian profile (as suggested by the numerical simulation) and the fits are also shown in Fig. 7 (solid lines). This figure clearly indicates that the efficiency of the focusing depends on the applied voltage (as expected). Increasing the voltage both decreases the width of the Gaussian and increases the height, i.e. the particles are more tightly focused. For the 40 nm particles, the area under the Gaussian curve also increases with increasing voltage, indicating that particles are being accumulated in the channel from outside the area of observation as the voltage is increased. However, as seen from the figures, focusing of these particles only begins at 10

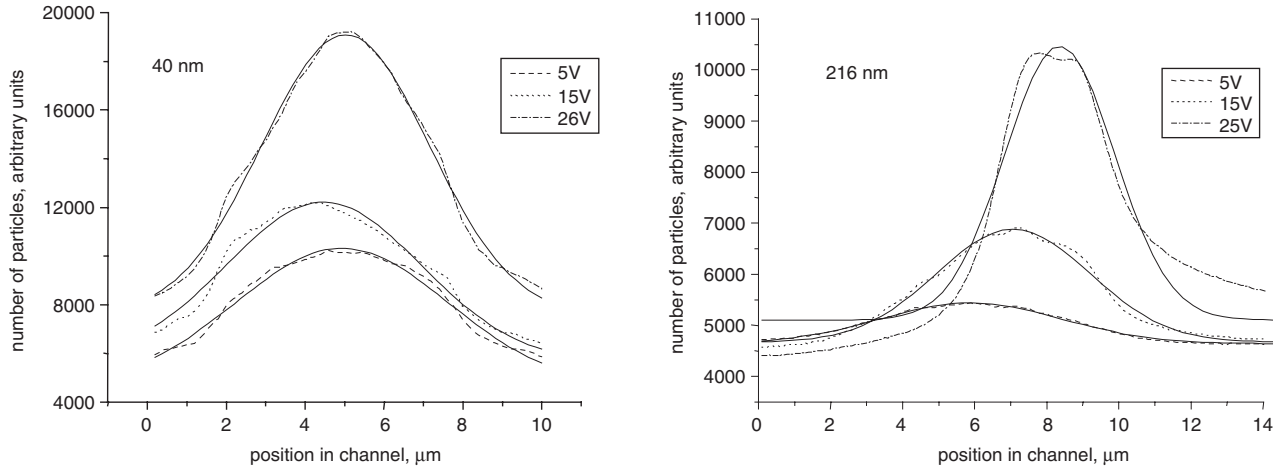


**Fig. 7** *Plots of average signal intensity (proportional to number of particles) obtained from images similar to those shown in Fig. 6 for two particle sizes and three voltages*
Also shown are Gaussian fits to this data

to 15 V. This probably indicates that the funnel section is less effective for these smaller particles. The 216 nm data shows a skewing of the peaks with voltage (also seen for the 460 nm beads, data not shown). This is due to imperfections in the fabricated chip, where the top and bottom set of electrodes were slightly offset from each other. This results in light being reflected from the very bright beads back into the camera. Also because the centre of the DEP focus is not coincident with the centre of the channel, as the voltage increases the midpoint of the stream of larger particles moves to one side.

Figure 8 shows the width of the Gaussian fits, plotted against voltage in a similar manner to that of Fig. 5, for the 40 nm, 216 nm and 460 nm diameter particles. Also plotted on the same graph for comparison, are the numerical results for the 216 nm particles. For the larger particles (216 and 460 nm), it is clear that increasing the voltage leads to a reduction in the width of the particle stream, i.e. an increase in focusing. The dotted lines represent exponential fits to the experimental data in the manner of Fig. 5. It can be seen that the trend mirrors the numerical data, but that the actual values are different by a factor of approximately 3. This could be due to limitations in the numerical model or a potential drop along the electrodes.

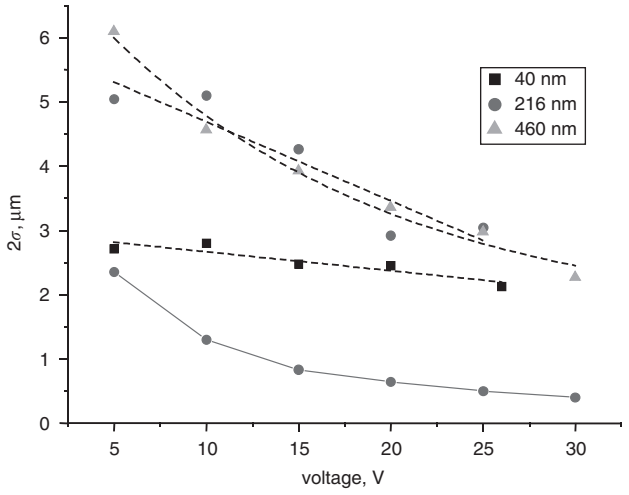


**Fig. 8** *Plot showing widths (2 σ) of Gaussian fits from Fig. 7 for three different particle sizes as function of applied voltage. Dashed lines are single exponential fits*
Also shown for comparison is numerical data taken from Fig. 5

The data for the 40 nm particles is different. There is almost a linear trend with increasing voltage. The images of Fig. 6 and 7 show that the width of the Gaussian hardly changes with voltage but there is a clear accumulation of particles in the channel. The fact that the focusing of these particles is less efficient is to be expected because in the high frequency limit, the DEP force on the 40 nm particles is 160 times less than on the 216 nm particles for the same applied voltage. To a first order approximation, reducing the channel and electrode gap by a factor of 5, to 2 μm, would restore the balance of forces and probably lead to extremely efficient focusing of 40 nm particles, and smaller. In addition the focusing of the 40 nm beads was performed at an applied frequency of 18 MHz. At this frequency, the Clausius–Mossotti factor for these particles is only 40% of the maximum value of −0.5, so that the DEP force is reduced proportionately. Frequencies in the 100 MHz region would be required to achieve a Clausius–Mossotti factor of –0.5 for latex beads of 100 nm or smaller.

## 5 Conclusions

We have designed and constructed a microfluidic chip capable of efficient focusing of nanoscale latex particles down to 40 nm diameter. Manipulation of smaller particles should be possible with the application of higher field frequencies, and also with devices of reduced geometry. DEP focusing has many advantages over electrokinetic focusing, which uses high-voltage DC fields. In particular, as we have shown, the particles remain focused as long as the electric field is applied. In contrast, DC electrokinetic focusing and other hydrodynamic focusing techniques operate by pinching fluid/particles at the intersection of two streams, and inevitably the particles diffuse out of the focused stream as they move away from the junction. DEP methods require that the particles are less polarisable than the suspending medium. This is relatively easy for latex particles and cells. We have made initial attempts to focus protein molecules such as FITC-labelled avidin. This has so far been inconclusive, probably due to the relatively low frequencies used. It is also not clear whether protein molecules would experience negative DEP, as the frequency dependent dielectrophoretic properties of proteins has not yet been fully investigated.

## 6 Acknowledgments

The authors would like to thank EPSRC for grant No GR/R28942/01 funding this work.

## 7 References

1 Fu, A.Y., Spence, C., Scherer, A., Arnold, F.H., and Quake, S.R.: 'A microfabricated fluorescence-activated cell sorter', *Nature Biotechnol.*, 1999, **17**, pp. 1109–1111
2 Schrum, D.P., Culbertson, C.T., Jacobson, S.C., and Ramsey, J.M.: 'Microchip flow cytometry using electrokinetic focusing', *Anal. Chem.*, 1999, **71**, pp. 4173–4177
3 Fu, A.Y., Spence, C., Scherer, A., Arnold, F.H., and Quake S. R.: 'An integrated microfabricated cell sorter', *Anal. Chem.*, 2002, **74**, pp. 2451–2457
4 Krüger, J., Singh, K., O'Neill, A., Jackson, C., Morrison, A., and O'Brien, P.: 'Development of a microfluidic device for fluorescence activated cell sorting', *J. Micromech. Microeng.*, 2002, **12**, pp. 486–494
5 Gawad, S., Schild, L., and Renaud, P.: 'Micromachined impedance spectroscopy flow cytometer for cell analysis and particle sizing', *Lab on a Chip*, 2001, **1**, pp. 76–82
6 Wolff, A., Perch-Nielsen, I.R., Larsen, U.D., Friis, P., Goranovic, G., Poulsen, C.R., Kutter, J.P., and Telleman, P.: 'Integrating advanced functionality in a microfabricated high-throughput fluorescent-activated cell sorter', *Lab on a Chip*, 2003, **3**, pp. 22–27
7 Sundararajan, N., Pio, M.S., Lee, L.P., and Berlin, A.: Three-dimensional hydrodynamic focusing in poly(dimethylsiloxane) (PDMS) microchannels for molecular detection. In Nanotech 2002: The 6th Annual European Conference On Micro & Nanoscale Technologies for the Biosciences, 2002, Montreux, Switzerland
8 Lee, G-W., Hung, C-I., Ke, B-J., Huang, G-R., Hwei, G-R., Hwei, B-H., and Lai, H-F.: 'Hydrodynamic focusing for a micromachined flow cytometer', *Trans. ASME J. Fluids Engin.*, 2001, **123**, pp. 672–679
9 Jacobson, S.C., and Ramsey, J.M.: 'Electrokinetic focusing in microfabricated channel structures', *Anal. Chem*, 1997, **69**, pp. 3212–3217
10 Chou, H-P., Spence, C., Scherer, A., and Quake, S.: 'A microfabricated device for sizing and sorting DNA molecules', *Proc. Natl. Acad. Sci. USA*, January 1999, **96**, pp. 11–13
11 Fiedler, S., Shirley, S.G., Schnelle, T., and Fuhr, G.: 'Dielectrophoretic sorting of particles and cells in a microsystem', *Anal. Chem.*, 1998, **70**, pp. 1909–1915
12 Müller, T., Gradl, G., Howitz, S., Shirley, S., Schnelle, T., and Fuhr, G.: 'A 3-D microelectrode system for handling and caging single cells and particles', *Biosens. Bioelectron.*, 1999, **14**, pp. 247–256
13 Schnelle, T., Müller, T., Fiedler, S. and Fohr, G.: 'The influence of higher moments on particle behaviour in dielectrophoretic field cages', *J. Electrostat.*, 1999, **46**, pp. 13–28
14 Morgan, H., Holmes, D., and Green, N.: 'AC electrokinetic focussing in microchannels: micro- and nano-particles'', *in* Morgan, H. (ed.): 'Electrostatics 2003' (IoP Publications, 2003)
15 Jones, T.B.: 'Electromechanics of Particles', (Cambridge University Press, Cambridge:, 1995)

# Microdevices for separation, accumulation, and analysis of biological micro- and nanoparticles

J. Kentsch, M. Dürr, T. Schnelle, G. Gradl, T. Müller, M. Jäger, A. Normann and M. Stelzle

**Abstract:** Microfabrication and performance of a novel microsystem for separation, accumulation and analysis of biological micro- and nanoparticles is reported. Versatile chip functions based on dielectrophoresis and microfluidics were integrated to isolate particles from complex sample solutions such as serum. A bead-based assay for virus detection is proposed. Separation of micro- and sub-μm beads employing dielectrophoretic deflector and bandpass structures is demonstrated. Individual antibody coated beads with hepatitis A virus bound to their surface were trapped by negative dielectrophoresis in a field cage and analysed by fluorescence microscopy.

## 1 Introduction

The basic principles of dielectrophoresis (DEP) and its application to biological materials have been established by Pohl [1] and Pethig [2]. The concept of DEP is particularly attractive as it enables non-contact manipulation of particles such as cells in solution by high frequency electric fields [3], and characterisation of their passive dielectric properties [4–8]. If 3D electrode arrays are employed, interaction with walls or unspecific adsorption of particles may be avoided. In addition, trapping of particles of interest in a femtolitre sized volume for analysis is also possible. DEP is compatible with biological fluids. A variety of different versatile functions such as separators, funnels and field-cages have already been established.

Dielectrophoretic forces scale with the volume of particles, i.e. $R^3$. This property may be used for the design of separation structures. However, decreasing particle size requires increasing strength and inhomogeneity of electric fields in order to generate sufficiently large forces to manipulate even sub-μm particles such as bacteria and viruses. Microfluidic systems with integrated micro- and nanoelectrode arrays enable generation of electric fields exceeding 100 kV/m without causing excessive heat dissipation. Suitable fabrication methods will be reported.

DEP has already successfully been employed to the manipulation of micro- and nanoparticles, for cell sorting and separation [9–17] single cell characterisation [15, 18–20], pathogen detection [21–23], in addition to manipulation and characterisation of viruses [24–30] and macromolecules [24, 31–34].



*IEE Proceedings* online no. 20031127

doi:10.1049/ip-nbt:20031127

Paper first received 23rd June 2003 and in revised form 24th October 2003

J. Kentsch, M. Dürr and M. Stelzle are with the Naturwissenschaftliches und Medizinisches Institut, Markwiesenstrasse 55, Reutlingen 72770, Germany

T. Schnelle and G. Gradl are with Evotec Technologies GmbH, Schnackenburgallee 114, Hamburg 22525, Germany

T. Müller is with the Institut für Biologie, Humboldt-Universität zu Berlin, Invalidenstrasse 42, Berlin 10115, Germany

M. Jäger is with the Fraunhofer-Institut für Biomedizinische Technik, Ensheimer Straße 48, St. Ingbert 66386, Germany

A. Normann is with Mediagnost GmbH, Aspenhaustraße 25, Reutlingen 72770, Germany

Technological approaches so far mostly relied on planar chips with 2D electrode arrangements in combination with hydrodynamic flux while there are relatively few reports of systems employing 3D arrays [24, 35–37].

## 2 Objective and concept

The aim of this research is to establish a versatile technology platform for contactless manipulation and analysis of biological micro- and, particularly, nanoparticles. For this purpose, a combination of dielectrophoretic deflector arrays, funnels and field-cages was integrated within a microfluidic device (Fig. 1). Since the performance of these individual function units may be externally tuned, the *NanoVirDetect* system may be adapted to a large variety of different sample compositions and properties. A dedicated system interface enables rapid simultaneous fluidic and electric interconnection of the system to peripheral units

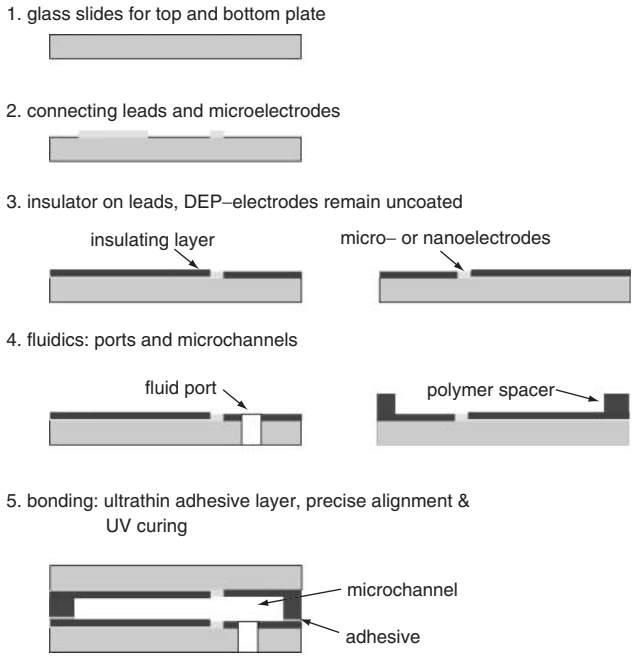


**Fig. 1** *Schematic depiction of manufacturing process*
The precision of the low temperature bonding process employing UV curable adhesive is particularly critical

16 Morgan, H., and Green, N.G.: '*AC Electrokinetics: Colloids and Nano-particles*' Pethig, R. (ed.): 2003, Baldock, UK: (Research Studies Press)
17 Schnelle, T., Muller, T., and Fuhr, G.: 'Trapping in AC octode field cages', *J. Electrostat.*, 2000, **50**, pp. 17–29
18 Castellanos, A., Ramos, A., González, A., Green, N.G., and Morgan, H.: 'Electrohydrodynamics and dielectrophoresis in microsystems: scaling laws', *J. Phys D Appl. Phys.*, 2003, **36**, pp. 2584–2597
19 Green, N.G., Ramos, A., and Morgan, H.: 'Numerical solution of the dielectrophoretic and travelling wave forces for interdigitated electrode arrays using the finite element method', *J. Electrostat.*, 2002, **56**, pp. 235–254
20 Langevin, P.: 'A theory of Brownian motion', *C.R. Acad. Sci.*, 1908, **146**, pp. 530–533
21 http://www.iee.org/proceedings/nbt